ACS OMEGA

Article

Cite This: ACS Omega 2018, 3, 2609−2617

High-Thermal-Stability and High-Thermal-Conductivity $Ti_3C_2T_x$ MXene/Poly(vinyl alcohol) (PVA) Composites

Rui Liu* and Weihua Li*

College of Chemical Engineering and Technology, Sun Yat-sen University, Tangjia Bay, Zhuhai 519082, People's Republic of China

ABSTRACT: MXenes, a new family of two-dimensional materials, have recently attracted increasing attention due to their unique properties for a wide range of potential applications. Herein, we synthesize $Ti_3C_2T_x$/poly(vinyl alcohol) (PVA) composites and investigate the effects of the thermal properties of MXene by temperature-dependent Raman spectroscopy and polarized-laser power-dependent Raman spectroscopy. Compared to the $Ti_3C_2T_x$ MXene, the PVA significantly improves the thermal stability of $Ti_3C_2T_x$ by reducing the thermal coefficient of the E_g^1 mode from −0.06271 to −0.03357 cm^{-1}/K, which is attributed to the strong Ti−O bonds formed between the MXene and PVA polymer confirmed by the X-ray photoelectron spectroscopy results. Meanwhile, the thermal conductivities of $Ti_3C_2T_x$ and $Ti_3C_2T_x$/PVA composites reach as high as about 55.8 and 47.6 W/(m K), respectively. Overall, this work will contribute to extend the MXene applications in terms of polymer-based nanocomposites and improve the reliability of the related devices effectively.

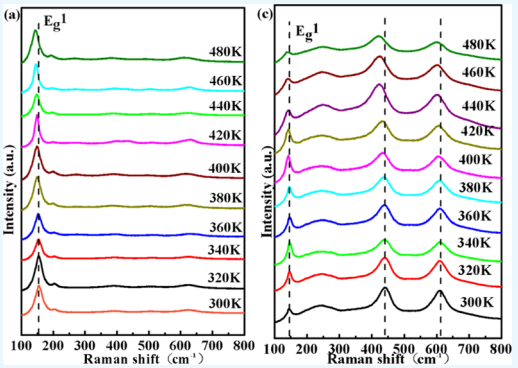

1. INTRODUCTION

Since the discovery of graphene, two-dimensional (2D) atomic crystals have attracted increasing scientific research interest owing to their high surface areas and unique properties that differ from the corresponding three-dimensional analogues.[1] Among these materials, MXenes, a recently discovered family of 2D transition-metal carbides or carbonitrides, shed new light on the development of energy conversion and storage devices.[2−6] Normally, MXenes are produced by the selective chemical etching of "A" elements (mostly Al or Si) from the layered ceramics called MAX phases.[7] The MAX phases are generally represented by the formula $M_{n+1}AX_n$, where M is an early transition metal, X is carbon and/or nitrogen, and n = 1, 2, or 3. Because MXenes are synthesized in fluoride-containing aqueous solutions, their surfaces are inevitably terminated with a mixture of −O, −F, and −OH groups.[8,9] Henceforth, these terminated MXenes will be labeled as $M_{n+1}X_nT_x$, where T represents the terminating groups and x is the number of terminating groups. MXenes are multilayered structures resembling those of exfoliated graphite and can be delaminated into single- or few-layer nanosheets, which dramatically increase the accessible surface.[10] Many members of the MXene family exhibit metallic conductivity, surface hydrophilicity, and excellent mechanical properties.[11−13] Furthermore, the optoelectronic properties of these materials can be finely tuned by changing the intercalation products between the MXene sublayers.[14] To date, MXenes have already been proved to be promising candidates for electrodes in lithium (Li)- and sodium (Na)-ion batteries[15−17] and supercapacitors,[18−20] as well as shown a great potential in the applications of water purification[21−23] and sensors.[24,25] In addition, theoretical studies suggest that several members of this family, such as Ti_2C and Mo_2C, can become potential candidates for hydrogen storage[26] and thermoelectric applications.[27] Meanwhile, MXenes can also be used to produce functional nanocomposites due to their functionalized surfaces and 2D morphology. The key factor to introduce polymer matrices into MXenes is the utilization of cationic-charged or hydrogen-bond-forming polymers to achieve a strong interaction with negatively charged OH/F/O-terminated MXene surface.[28] Pre-Previously, $Ti_3C_2T_x$ MXene was attempted to mix with charged diallyldimethylammonium chloride, polydiallyldimethylammonium, electrically neutral poly(vinyl alcohol) (PVA), or polyacrylamide (PAM) to produce $Ti_3C_2T_x$/polymer nanocomposite systems.[28,29] Using dimethylsulfoxide, uniform and flexible $Ti_3C_2T_x$/PAM composites with only 6 wt % (1.7 vol %) MXene loading were obtained with an electrical conductivity of about 3.3×10^{-2} S/m.[30] Ling et al. reported that the $Ti_3C_2T_x$/PVA composites showed electrical conductivity as high as 2.2×10^4 S/m, whereas the measured electrical conductivity of pure $Ti_3C_2T_x$ films was about 2.4×10^5 S/m.[28] In addition, the tensile strength of the $Ti_3C_2T_x$/PVA composites was significantly enhanced from 22 ± 2 to 91 ± 10 MPa compared to the pure $Ti_3C_2T_x$ films. The introduction and confinement of the polymer between the MXene flakes not only increased flexibility, but also stimulated cationic intercalation, offering an impressive volumetric capacitance of ∼530 F/cm^3 for MXene/PVA−KOH composite films at 2 mV/s. This implies that MXenes are promising fillers in multifunctional polymer composites, which in turn can be employed in many

Received: December 16, 2017
Accepted: February 21, 2018
Published: March 5, 2018

DOI: 10.1021/acsomega.7b02001
ACS Omega 2018, 3, 2609−2617

applications such as flexible and wearable energy-storage devices, radio frequency shielding, water filtration system, and so on. Raman spectroscopy, a nondestructive method, is typically used to investigate the strain distribution and thermal stability of a material by assessing its Raman frequency shifts and related thermal coefficients.[31,32] In light of the importance of MXene/polymer composite systems, in this study, we fabricated uniform $Ti_3C_2T_x$/PVA composites and explored their thermal stability and thermal conductivity by temperature-dependent and polarized-laser power-dependent Raman measurements. The results demonstrate that the introduction of PVA significantly improves the thermal stability of the composites in comparison to the pure $Ti_3C_2T_x$. Meanwhile, the thermal conductivity of $Ti_3C_2T_x$/PVA composites also stays at high level. These results will have a great impact on the reliability of the related devices.

2. EXPERIMENTAL SECTION

Figure 1 provides a general overview of the fabrication process of $Ti_3C_2T_x$/PVA composites. A piece of the Ti_3AlC_2 monolith

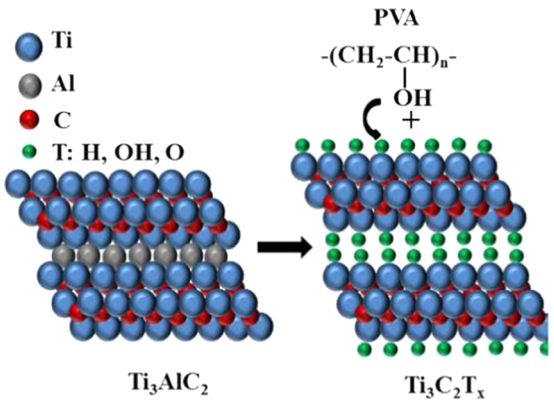

Figure 1. Schematic diagram of the fabrication process of $Ti_3C_2T_x$/PVA composites.

(1 g) was immersed into 10 mL of 50 wt % hydrofluoric acid solution for 18 h at room temperature to dissolve the Al atoms. The resulting suspension of multilayered $Ti_3C_2T_x$ was repeatedly washed with deionized water six to eight times, centrifuged at 1500 rpm for 10 min, and decanted until the supernatant reached a pH of ~6. The separated wet sediment was dried under vacuum for 24 h before further experiments. PVA with a molecular weight of about 67 000 g/mol in 1 wt % aqueous solutions was prepared. The $Ti_3C_2T_x$ MXene solution (1 g/500 mL water) was put into the PVA solutions. The weight ratio of $Ti_3C_2T_x$ to PVA can be adjusted by their initial weights. The combined mixture was vortexed for 1 h, then sonicated for 30 min at the power of 100 W until the solution attained visual homogeneity, and centrifuged at 1500 rpm for 10 min. Finally, the $Ti_3C_2T_x$/PVA wet sediment was dried at 60 °C under vacuum for 24 h and the residual was the $Ti_3C_2T_x$/PVA composites. The $Ti_3C_2T_x$/PVA composite film was obtained by filtration through poly(vinylidene difluoride) membrane and dried in vacuum at room temperature.

A powder X-ray diffractometer (XRD, Bruker, D8 Advance) with Cu Kα radiation (λ = 0.15406 nm) was used to obtain the X-ray powder diffraction patterns for the Ti_3AlC_2, pristine $Ti_3C_2T_x$ MXene, and $Ti_3C_2T_x$/PVA composites. The morphologies of the $Ti_3C_2T_x$ MXene and $Ti_3C_2T_x$/PVA composites were characterized by a scanning electron microscope (SEM) (Hitachi SU-70) and a transmission electron microscope (TEM) (Tecnai G2 F20 S-Twin) operated at an accelerating voltage of 200 kV. Thermogravimetric analysis was performed by a thermal gravimetric analyzer (Netzsch, TG 209F1) in nitrogen atmosphere and oxygen atmosphere. The heating rate was 10 K/min. Raman spectroscopy measurements were carried out in a confocal microscopy setup with a 532 nm solid-state green laser for excitation. The temperature ranging from 300 K (room temperature) to 480 K was controlled by a heating stage. Polarized-laser power-dependent Raman measurements were performed at $0.01P_0$, $0.1P_0$, $0.25P_0$, $0.5P_0$, $0.75P_0$, and P_0, where P_0 = 2.5 mW. And thermal conductivities of the pristine $Ti_3C_2T_x$ MXene and $Ti_3C_2T_x$/PVA composites were also confirmed by a laser thermal conductivity test instrument (Netzsch, LFA 427) at room temperature. X-ray photoelectron spectroscopy (XPS) studies were carried out in a VG ESCALAB 220i-XL system equipped with a monochromatized Al Kα X-ray source (1486.6 eV), a multichannel plate, and a delay-line detector under a vacuum of 1×10^{-9} mbar. High-resolution (HR) spectra were collected at a constant pass energy of 20 eV and quantified using empirically derived relative sensitivity factors provided by Kratos Analytical. Binding energies were referenced to the C 1s peak of the C−C bond at 284.80 eV. The data were analyzed by commercially available software CasaXPS.

3. RESULTS AND DISCUSSION

Figure 2 shows the XRD patterns of Ti_3AlC_2, as-prepared $Ti_3C_2T_x$ powders, and the corresponding $Ti_3C_2T_x$/PVA

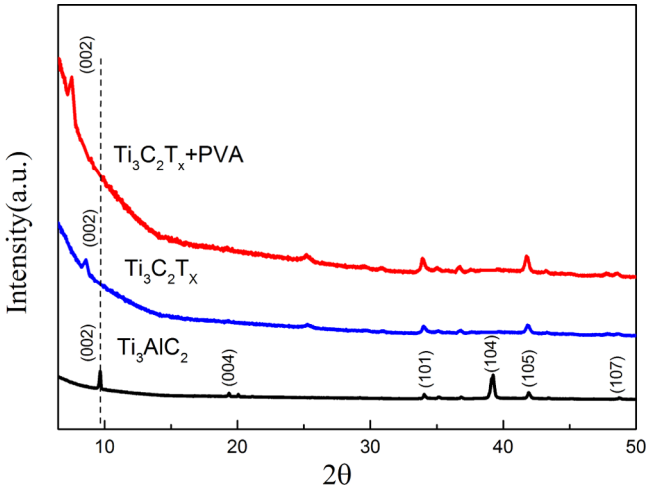

Figure 2. XRD patterns of Ti_3AlC_2, $Ti_3C_2T_x$ MXene, and $Ti_3C_2T_x$/PVA composites.

composites. It can be readily observed that the (002) peak of the Ti_3AlC_2 MAX phase shifts toward lower angles from about 9.60−8.60° ($Ti_3C_2T_x$ MXene) and 7.80° ($Ti_3C_2T_x$/PVA composites), which indicated the increase of the c lattice parameter. According to the Bragg formula $2d \sin\theta = n\lambda$, where θ is the Bragg angle, d is the interplanar spacing, and λ is the wavelength of the incident X-ray (0.15406 nm), the d parameters of the Ti_3AlC_2 MAX, $Ti_3C_2T_x$ MXene, and $Ti_3C_2T_x$/PVA composites are about 18.34, 20.54, and 22.10 Å, respectively. This demonstrates that the PVA can interact with $Ti_3C_2T_x$ MXene. The surface functional groups of MXene are changed, which enlarges the d-spacing of MXene sheets. In

DOI: 10.1021/acsomega.7b02001
ACS Omega 2018, 3, 2609−2617

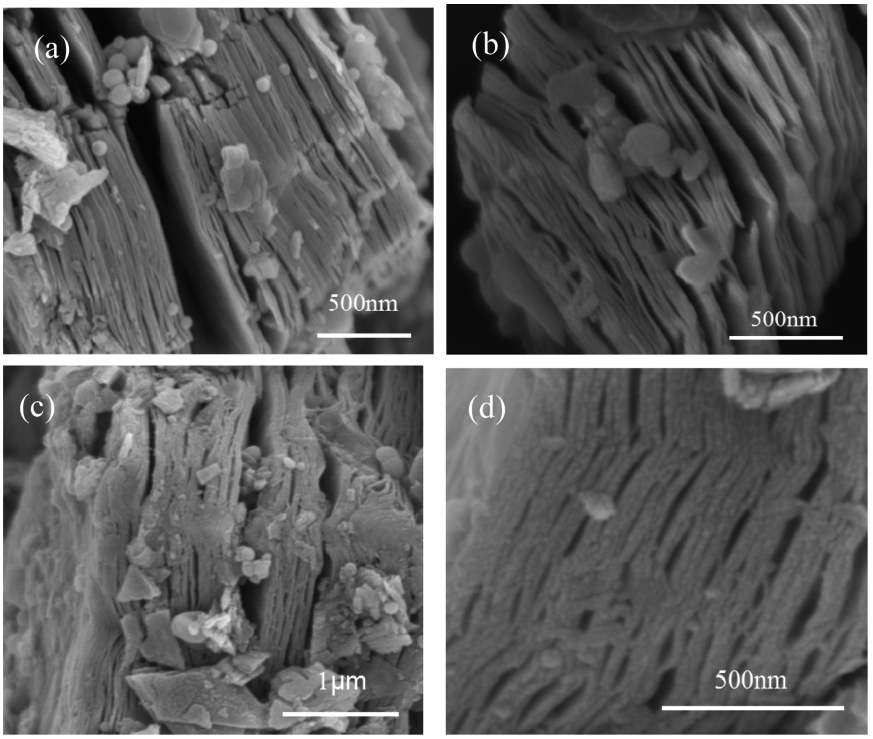

Figure 3. (a) SEM image of $Ti_3C_2T_x$ MXene, (b) enlarged view of (a), (c) SEM images of $Ti_3C_2T_x$/PVA, and (d) enlarged view of (c).

addition, the broadening of the (002) peaks in the $Ti_3C_2T_x$ MXene compared to that in the MAX phase mainly attributes to the decreasing structure order.[11]

The as-synthesized $Ti_3C_2T_x$ has a layered morphology resembling exfoliated graphite, as shown in Figure 3a. The enlarged view of $Ti_3C_2T_x$ (Figure 3b) indicates the clear layered structure. However, in Figure 3c, after introduction of PVA, the sheets stack together because the hydroxyl in the PVA reacted with the −OH-terminated MXene surface (−OH + −OH = −O− + H_2O) and formed Ti−O bonds at the surface, which is confirmed by the XPS results. The enlarged view of $Ti_3C_2T_x$/PVA composites (Figure 3d) indicates compact layered structure. To further explore the structure changes of $Ti_3C_2T_x$ MXene after the PVA reaction, the material is also characterized by TEM, as displayed in Figure 4. Figure 4a,d exhibit the two-dimensional nanosheets of $Ti_3C_2T_x$ and $Ti_3C_2T_x$/PVA, respectively. The exfoliated slices are very thin and disperse as single layer or stack of several layers. The inset selected area electron diffraction (SAED) patterns in Figure 4b,e show that the crystal planes of the MXenes are hexagonal systemic, indicating that the PVA does not change the crystal type. Furthermore, the space parameters of both the $Ti_3C_2T_x$ and $Ti_3C_2T_x$/PVA composites corresponding to $(10\bar{1}0)$ planes are measured to be about 0.2656 and 0.2595 nm, respectively. On the basis of the above values, the lattice constant *a* is about 0.3070 nm for $Ti_3C_2T_x$ and 0.2982 nm for $Ti_3C_2T_x$/PVA. Therefore, it demonstrates that the original basal plane structure of the $Ti_3C_2T_x$ MXene shrinks a little after the PVA treatment coupled with the lattice expansion along the *c* axis. Figure 4c,f shows the cross sections of the multilayered $Ti_3C_2T_x$ MXene and $Ti_3C_2T_x$/PVA composites, respectively. The nanosheets are stacked less uniformly in $Ti_3C_2T_x$/PVA than in $Ti_3C_2T_x$ due to the polymer reaction.

Figure 5a shows the TG curve of $Ti_3C_2T_x$ in nitrogen atmosphere. The temperature is from room temperature to 950 °C. There are three weight-change steps. The first step is due to the release of free water adsorbed on the surface of $Ti_3C_2T_x$. The second step is due to the release of bonding water and functional groups on the surface of $Ti_3C_2T_x$. The third step is due to the decomposition of $Ti_3C_2T_x$ MXene. The decomposition temperature of pure $Ti_3C_2T_x$ MXene is about 785 °C. Figure 5b shows the TG curve of $Ti_3C_2T_x$/PVA composites in nitrogen atmosphere. The temperature is also from room temperature to 950 °C. There are four weight-change steps compared to $Ti_3C_2T_x$ MXene. The temperature from 220 to 480 °C is the decomposition temperature of PVA. The content of PVA is 12.71% in the composites in our experiment. The decomposition temperature of $Ti_3C_2T_x$/PVA composites is about 823 °C, which is higher than that of $Ti_3C_2T_x$ MXene. So, the thermal stability of $Ti_3C_2T_x$/PVA composites is better than that of $Ti_3C_2T_x$ MXene in nitrogen atmosphere. Figure 5c shows the TG curve of $Ti_3C_2T_x$ in oxygen atmosphere. The temperature is from room temperature to 950 °C. There are four weight-change steps. We note that from 322 to 729 °C, the mass increases 19.98%, which is due to the oxidation of MXene. The oxidation temperature of $Ti_3C_2T_x$ MXene is about 322 °C, and the decomposition temperature of MXene is about 729 °C. Figure 5d shows the TG curve of $Ti_3C_2T_x$/PVA composites in oxygen atmosphere. The temperature is from room temperature to 950 °C. There are five weight-change steps. The oxidation temperature of the composites is about 530 °C, and the decomposition temperature of the composites is about 811 °C. The result indicates a better thermal stability of $Ti_3C_2T_x$/PVA composites than pure $Ti_3C_2T_x$ MXene in oxygen atmosphere. So, from our TG results, the introduction of PVA can improve the thermal stability of $Ti_3C_2T_x$ in both nitrogen and oxygen atmosphere.

Raman spectroscopy is a powerful tool to investigate the atomic bonds, thermal stability, and thermal conductivity of two-dimensional materials, such as black phosphorus, MoS_2,

DOI: 10.1021/acsomega.7b02001
ACS Omega 2018, 3, 2609−2617

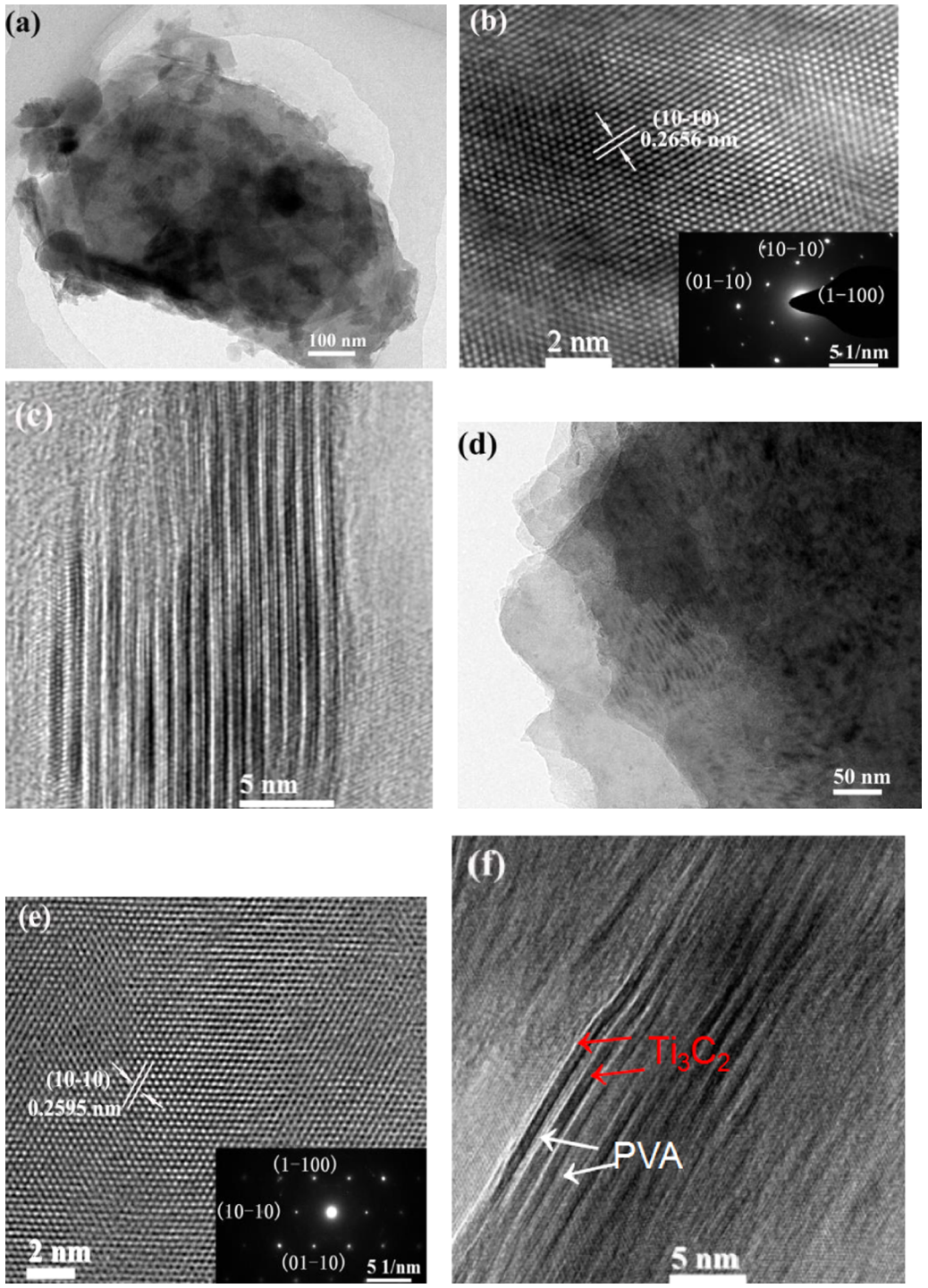

Figure 4. (a, c) TEM images, (b) HRTEM image of $Ti_3C_2T_x$ MXene (inset: the corresponding SAED pattern), (d, f) TEM images, (e) HRTEM image of $Ti_3C_2T_x$/PVA composites (inset: the corresponding SAED pattern).

graphene, and so on.[33−35] In this work, temperature-dependent Raman measurements ranging from 300 to 480 K were carried out for both $Ti_3C_2T_x$ MXenes and $Ti_3C_2T_x$/PVA composites. Raman frequency spectra with increasing temperature are plotted in Figure 6a,c. In $Ti_3C_2T_x$, the Raman frequency of about 156 cm^{-1} (E_g^1 mode) at room temperature is mainly from the in-plane vibrations of Ti2 and C atoms, as illustrated in Figure 6e. Besides, the Raman peaks at 606 cm^{-1} (E_g^2 mode) and 440 cm^{-1} in the $Ti_3C_2T_x$/PVA composite are attributed to the in-plane vibrations of C and O atoms, respectively. However, the E_g^1 mode shifts to a lower wave number at about 146.4 cm^{-1} in the $Ti_3C_2T_x$/PVA composite. It can be inferred that the PVA polymer weakens the in-plane motion of the Ti2 and C atoms. In comparison to the bare Ti_3C_2 nanosheet, the T-terminated Ti_3C_2 normally has a smaller *a* parameter and a larger *d* spacing while the atoms remain in the same Wyckoff positions. The XRD and TEM results have demonstrated that the *c* and *a* lattice parameters are enlarged about 1.56 Å and reduced 0.088 Å, respectively, after the PVA treatment. As a result, the Ti2 atoms are pushed

DOI: 10.1021/acsomega.7b02001
ACS Omega 2018, 3, 2609−2617

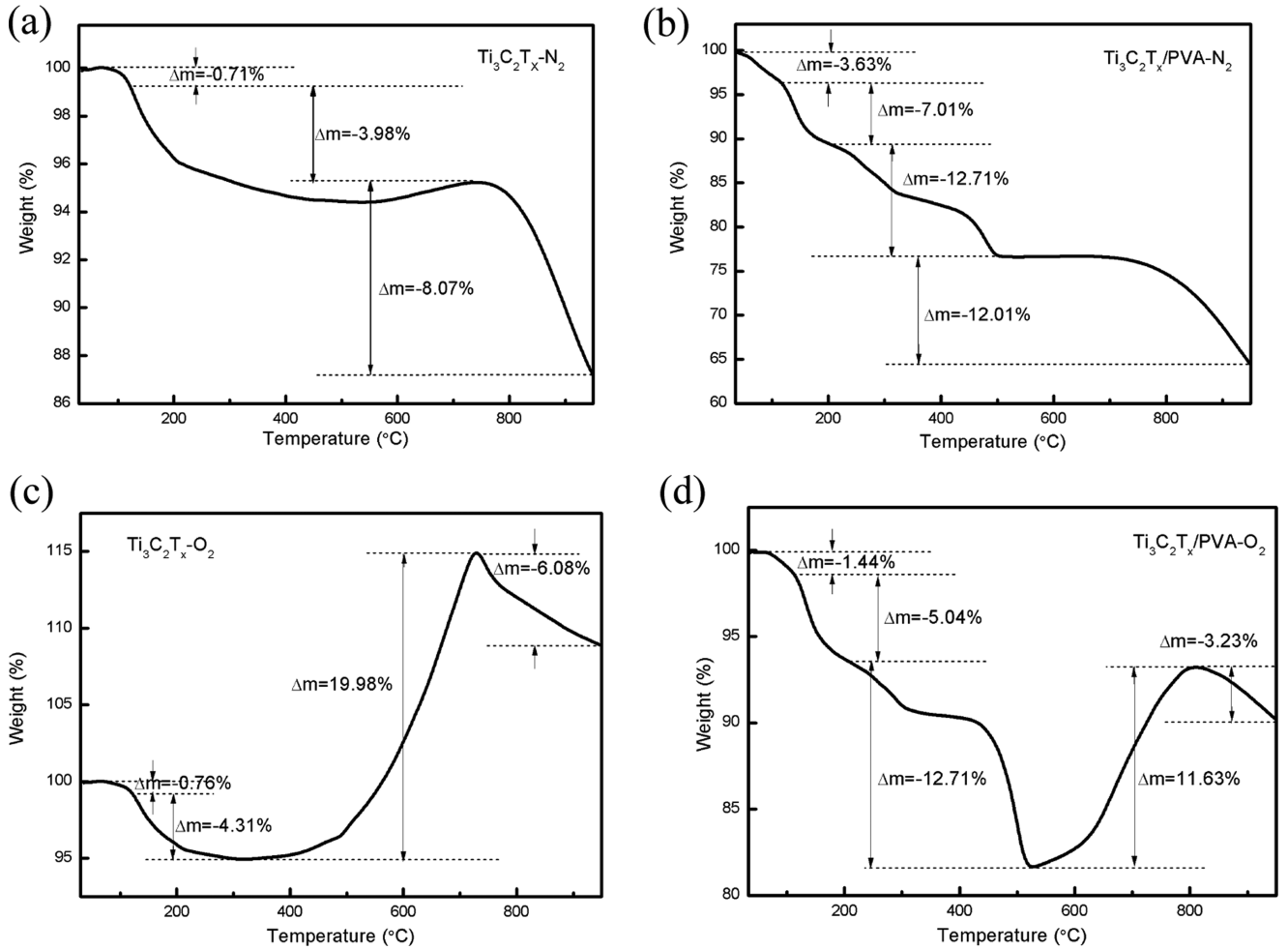

Figure 5. TG curves of (a) $Ti_3C_2T_x$ and (b) $Ti_3C_2T_x$/PVA composites in nitrogen atmosphere and (c) $Ti_3C_2T_x$ and (d) $Ti_3C_2T_x$/PVA composites in oxygen atmosphere.

out a little from the plane, then the bond length between the Ti1 and C atoms shrinks, whereas that between the Ti2 and C atoms is elongated, and in turn weakens the in-plane vibrations of Ti2 and C atoms. From Figure 6b,d, the Raman phonon mode E_g^1 obviously exhibits red shift from 300 to 480 K and can be fitted by a linear equation: $\omega = \omega_0 + \chi\Delta T$, where ω_0 is the mode frequency at room temperature, χ is the first-order temperature coefficient, and ΔT is the temperature difference relative to 300 K. The measured χ value for the $Ti_3C_2T_x$/PVA composites is about -0.03357 ± 0.00023 cm^{-1}/K, which is much smaller than the corresponding value -0.06271 ± 0.00045 cm^{-1}/K of the $Ti_3C_2T_x$ MXenes, indicating a better thermal stability in the former. Several data point dispersions are attributed to slight variation in the laser spot focused on the material. The observed softening of the Raman peaks with increasing temperature arises from an anharmonicity, which is related to the harmonic potential constant, the phonon occupation, as well as the thermal expansion of the crystal.[36] The improvement of thermal stability in the $Ti_3C_2T_x$/PVA composites is primarily contributed to the surface modification introduced by the PVA treatment. Therefore, it is essential to explore the change of the chemical bonding.

XPS investigations were performed to characterize the chemical compositions of the prepared MXene powders and composites. A detailed survey spectrum for both samples shows the presence of Ti, oxygen (O), fluorine (F), and carbon (C) (not shown here). The relative high-resolution XPS images of Ti 2p and O 1s are shown in Figure 7. The Ti 2p component centered at 455.9 eV is associated with the Ti−C bonds, whereas that at about 461 eV can be assigned to the Ti−O and Ti−F bonds, which are totally referred as $Ti-O_xF_y$.[37,38] Compared to the pure $Ti_3C_2T_x$ MXene, the peak integrated intensity ratio of $Ti-O_xF_y$ to Ti−C increases from about 0.425 to 0.693 in the $Ti_3C_2T_x$/PVA composite, which indicates that more $Ti-O_xF_y$ bonds are formed after PVA intercalation. Similarly, the O 1s XPS images with Ti−O bond at about 529.0 eV, Ti−OH bond at 532.0 eV,[39] and C−O bond at 533.1 eV are presented in Figure 7b,d. The intensity ratio of Ti−O bond to Ti−OH bond is about 0.657 in $Ti_3C_2T_x$ MXene, whereas that in the $Ti_3C_2T_x$/PVA composites increases to about 0.859, which indicates that more Ti−O bonds are formed after the PVA treatment. The result is consistent with the results of Ti 2p XPS. Overall, the PVA polymer can conjugate with the $Ti_3C_2T_x$ MXene effectively in terms of −Ti−O bond forming $Ti_3C_2T_x$/PVA composites. In $Ti_3C_2T_x$ MXenes, the bond lengths of Ti−O, Ti−F, and Ti−OH are 1.97, 2.17, and 2.19 Å, respectively, indicating that Ti−O bond is the most stable one among the terminated groups.[40] Generally, the strong terminal Ti−O bond significantly weakens the vibrations in which the surface Ti atoms are involved and increases the material thermal stability greatly, especially in the $Ti_3C_2T_x$/PVA composites where the PVA polymer profoundly increases the

DOI: 10.1021/acsomega.7b02001
ACS Omega 2018, 3, 2609−2617

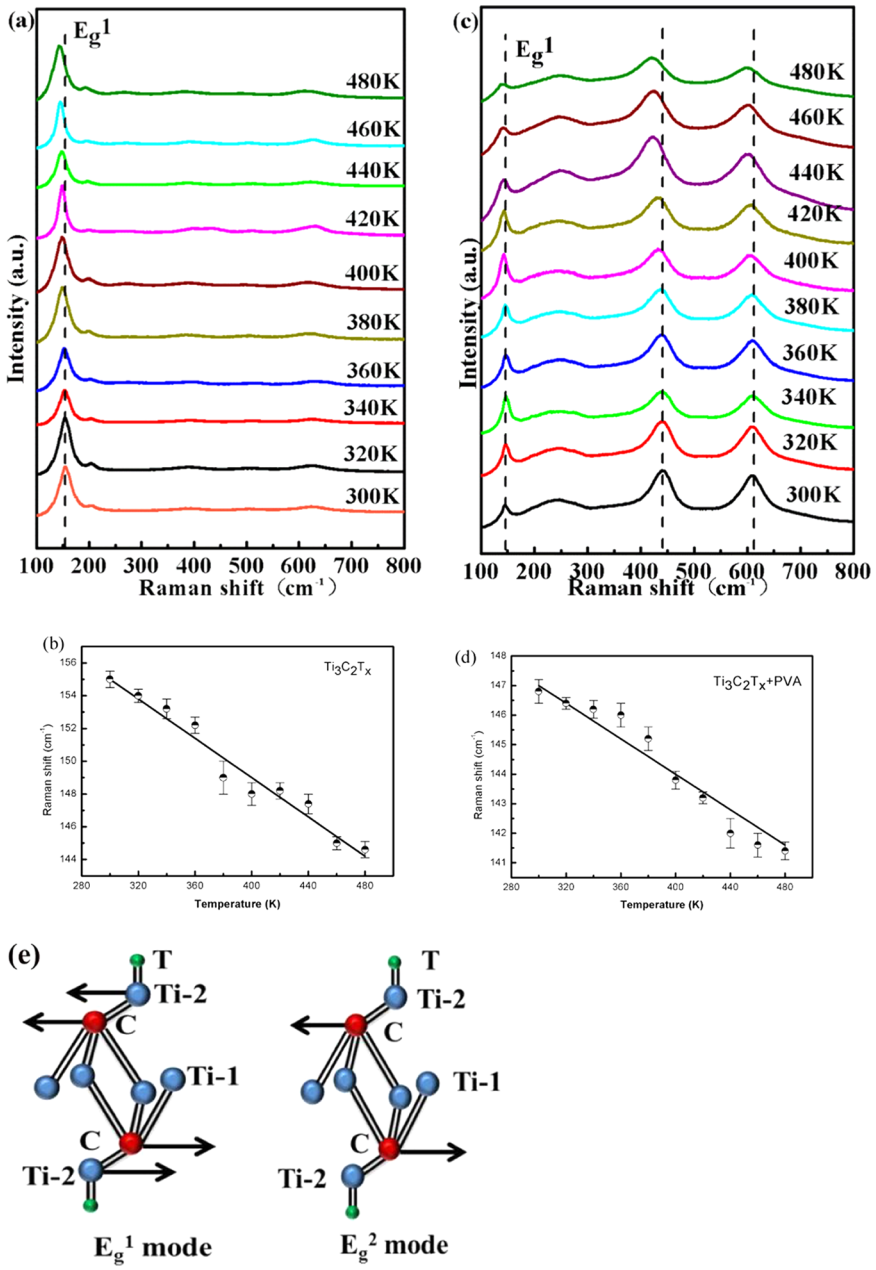

Figure 6. Temperature-dependent Raman spectra of (a) $Ti_3C_2T_x$ MXene and (c) $Ti_3C_2T_x$/PVA composites from 300 to 480 K. (b, d) Corresponding plots of Raman mode frequency versus temperature including a linear fit. (e) Schematic illustration of the Raman modes.

relative intensity of Ti−O bond declared by the XPS results. Otherwise, one PVA molecular $(C_2H_4O)_n$ includes much −OH groups, which promotes PVA polymer cladding on the $Ti_3C_2T_x$ MXene effectively. This is also helpful to improve the thermal stability and prevent $Ti_3C_2T_x$ MXene from oxidation and rolling into conical shape. Thus, the PVA polymer has great impacts on the thermal properties of MXenes, and it is reasonable to assume that it would be possible to tune the thermal stability or thermal conductivity of the $Ti_3C_2T_x$/PVA composites by controlling the $Ti_3C_2T_x$-to-PVA ratio.

To obtain the thermal conductivity, polarized-laser power-dependent Raman spectra were recorded, as displayed in Figure 8a,b. The maximum laser power P_0 was about 2.5 mW measured at the exit of the microscope lens and can be reduced using an optical attenuator. Obvious frequency red shift of the Raman peaks with increasing laser power was discovered, which arose from the local laser heating effect. Figure 8c,d show the red shift of the E_g^1 mode frequency derived from the power-dependent Raman spectra. The $\partial\omega/\partial p$ coefficients for the $Ti_3C_2T_x$ MXene and $Ti_3C_2T_x$/PVA composite films are about 968 and 1081 cm^{-1}/W, respectively. For two-dimensional materials with thin-film structure, the thermal conductivity can be expressed as

$$k = \chi(1/2\pi h)(\partial\omega/\partial p)^{-1} \quad (1)$$

where χ is the first temperature coefficient of the E_g^1 for the $Ti_3C_2T_x$ MXene and $Ti_3C_2T_x$/PVA composite films and h is the thickness of the film. Taking the related values into eq 1, the thermal conductivities of the $Ti_3C_2T_x$ and $Ti_3C_2T_x$/PVA composite films are about 55.8 and 47.6 W/(m K), respectively.

To confirm the thermal conductivity results, the laser flash method was also performed. The samples were cut into circular

DOI: 10.1021/acsomega.7b02001
ACS Omega 2018, 3, 2609−2617

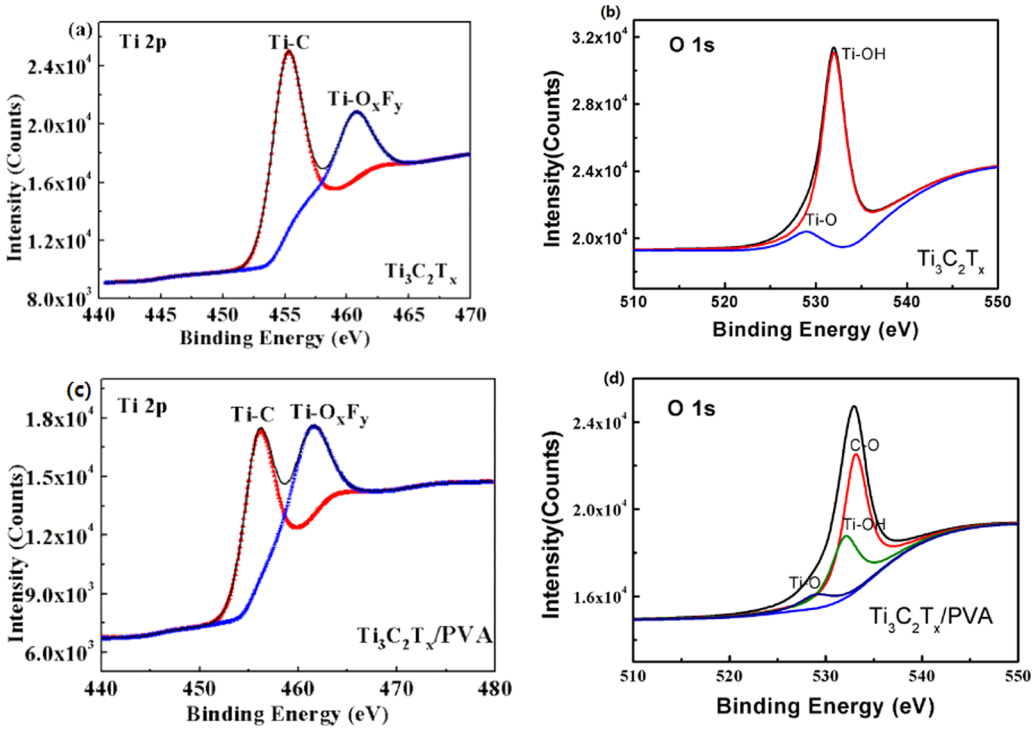

Figure 7. High-resolution Ti 2p and O 1s XPS images of (a, b) $Ti_3C_2T_x$ MXene and (c, d) $Ti_3C_2T_x$/PVA composite.

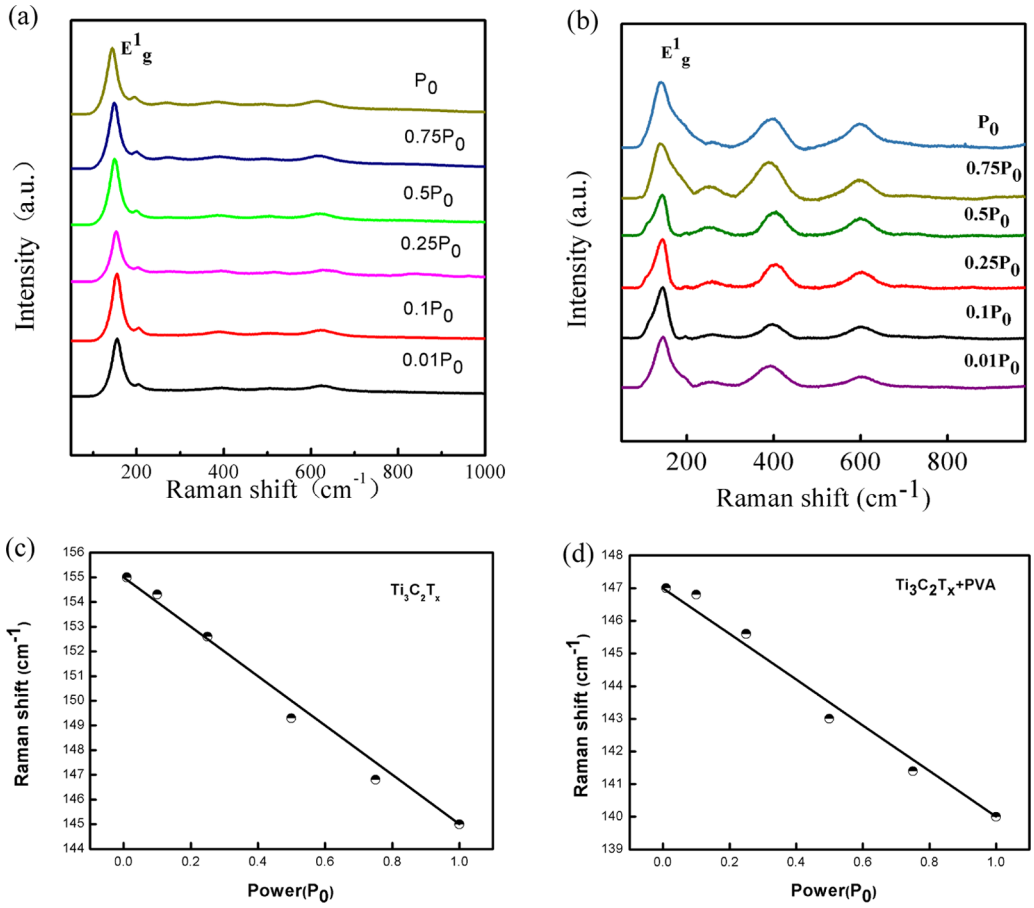

Figure 8. Polarized-laser power-dependent Raman spectra of (a) $Ti_3C_2T_x$ MXene and (b) $Ti_3C_2T_x$/PVA composite films under different laser power. Power dependence of E_g^1 mode of (c) $Ti_3C_2T_x$ MXene and (d) $Ti_3C_2T_x$/PVA composite films including linear fits of the experimental data.

DOI: 10.1021/acsomega.7b02001
ACS Omega 2018, 3, 2609−2617

specimens with a diameter of 20 mm and a thickness of 3 mm. The experiments were carried at room temperature. The thermal conductivities of the $Ti_3C_2T_x$ and $Ti_3C_2T_x$/PVA composite films are tested for 55.2 ± 1.7 and 47.3 ± 1.2 W/(m K), respectively, which are in accordance with the polarized-laser power-dependent Raman test results. With the introduction of PVA, the conductivity of the $Ti_3C_2T_x$/PVA composites decreases little from pure $Ti_3C_2T_x$ MXene. And the conductivity of the $Ti_3C_2T_x$/PVA composites can still surpass that of Fe (47.4 W/(m K)), SiO_2 (7.6 W/(m K)), Al_2O_3 (45 W/(m K)), stainless steel (40 W/(m K)), and most of the other two-dimensional materials. Our results show that the $Ti_3C_2T_x$/PVA composites exhibit high thermal stability and thermal conductivity and can be used in many areas, such as supercapacitors, Li-ion batteries, solar cells, electromagnetic shielding, and so on.

4. SUMMARY

In conclusion, high-thermal-stability and high-thermal-conductivity $Ti_3C_2T_x$/PVA composites is prepared in our work. The effects of PVA polymer on the thermal properties of $Ti_3C_2T_x$ MXene are investigated. The PVA polymer significantly improves the thermal stability of the MXene by introducing strong Ti−O bonds and cladding on the surface of the $Ti_3C_2T_x$ MXene without changing the crystal structure largely. The thermal conductivities of $Ti_3C_2T_x$ and $Ti_3C_2T_x$/PVA are about 55.8 and 47.6 W/(m K), respectively, which are even higher than those of some metals and most of the other two-dimensional materials. This study makes a crucial step to explore the potential use of MXene in polymer-based nanocomposites for a host of applications (e.g., energy-storage devices, water filtration system, thermoelectric devices, and Aeronautics and Astronautics materials) in harsh environment.

AUTHOR INFORMATION

Corresponding Authors

*E-mail: lrsnld@hotmail.com (R.L.).
*E-mail: 1685680@163.com (W.L.).

ORCID

Rui Liu: 0000-0002-0719-953X

Author Contributions

The paper was written through contributions of all authors. All authors have given approval to the final version of this paper.

Notes

The authors declare no competing financial interest.

ACKNOWLEDGMENTS

The authors gratefully acknowledge the financial support of National Nature Science Foundation of China (51525903), the AoShan Talents Outstanding Scientist Program Supported by Qingdao National Laboratory for Marine Science and Technology (2017ASTCP-OS09).

REFERENCES

(1) Ferrari, A. C.; Bonaccorso, F.; Fal'ko, V.; Novoselov, K. S.; Roche, S.; Boggild, P.; Borini, S.; Koppens, F. H. L.; Palermo, V.; Pugno, N.; Garrido, J. A.; Sordan, R.; Bianco, A.; Ballerini, L.; Prato, M.; Lidorikis, E.; Kivioja, J.; Marinelli, C.; Ryhanen, T.; Morpurgo, A.; Coleman, J. N.; Nicolosi, V.; Colombo, L.; Fert, A.; Garcia-Hernandez, M.; Bachtold, A.; Schneider, G. F.; Guinea, F.; Dekker, C.; Barbone, M.; Sun, Z. P.; Galiotis, C.; Grigorenko, A. N.; Konstantatos, G.; Kis, A.; Katsnelson, M.; Vandersypen, L.; Loiseau, A.; Morandi, V.; Neumaier, D.; Treossi, E.; Pellegrini, V.; Polini, M.; Tredicucci, A.; Williams, G. M.; Hong, B. H.; Ahn, J. H.; Kim, J. M.; Zirath, H.; van Wees, B. J.; van der Zant, H.; Occhipinti, L.; Di Matteo, A.; Kinloch, I. A.; Seyller, T.; Quesnel, E.; Feng, X. L.; Teo, K.; Rupesinghe, N.; Hakonen, P.; Neil, S. R. T.; Tannock, Q.; Lofwander, T.; Kinaret, J. Science and technology roadmap for graphene, related two-dimensional crystals, and hybrid systems. *Nanoscale* **2015**, *7*, 4598−4810.

(2) Magne, D.; Mauchamp, V.; Celerier, S.; Chartier, P.; Cabioc'h, T. Spectroscopic evidence in the visible-ultraviolet energy range of surface functionalization sites in the multilayer Ti_3C_2 MXene. *Phys. Rev. B* **2015**, *91*, No. 201409.

(3) Mashtalir, O.; Lukatskaya, M. R.; Zhao, M. Q.; Barsoum, M. W.; Gogotsi, Y. Amine-Assisted Delamination of Nb2C MXene for Li-Ion Energy Storage Devices. *Adv. Mater.* **2015**, *27*, 3501−3506.

(4) Peng, Y. Y.; Akuzum, B.; Kurra, N.; Zhao, M. Q.; Alhabe, M.; Anasori, B.; Kumbur, E. C.; Alshareef, H. N.; Ger, M. D.; Gogotsi, Y. All-MXene (2D titanium carbide) solid-state microsupercapacitors for on-chip energy storage. *Energy Environ. Sci.* **2016**, *9*, 2847−2854.

(5) Xia, Q. X.; Fu, J. J.; Yun, J. M.; Mane, R. S.; Kim, K. H. High volumetric energy density annealed-MXene-nickel oxide/MXene asymmetric supercapacitor. *RSC Adv.* **2017**, *7*, 11000−11011.

(6) Xie, X. Q.; Zhao, M. Q.; Anasori, B.; Maleski, K.; Ren, C. E.; Li, J. W.; Byles, B. W.; Pomerantseva, E.; Wang, G. X.; Gogotsi, Y. Porous heterostructured MXene/carbon nanotube composite paper with high volumetric capacity for sodium-based energy storage devices. *Nano Energy* **2016**, *26*, 513−523.

(7) Naguib, M.; Gogotsi, Y. Synthesis of Two-Dimensional Materials by Selective Extraction. *Acc. Chem. Res.* **2015**, *48*, 128−135.

(8) Wang, H. W.; Naguib, M.; Page, K.; Wesolowski, D. J.; Gogotsi, Y. Resolving the Structure of Ti3C2Tx MXenes through Multilevel Structural Modeling of the Atomic Pair Distribution Function. *Chem. Mater.* **2016**, *28*, 349−359.

(9) Naguib, M.; Kurtoglu, M.; Presser, V.; Lu, J.; Niu, J. J.; Heon, M.; Hultman, L.; Gogotsi, Y.; Barsoum, M. W. Two-Dimensional Nanocrystals Produced by Exfoliation of Ti3AlC2. *Adv. Mater.* **2011**, *23*, 4248−4253.

(10) Chang, F. Y.; Li, C. S.; Yang, J.; Tang, H.; Xue, M. Q. Synthesis of a new graphene-like transition metal carbide by de-intercalating Ti_3AlC_2. *Mater. Lett.* **2013**, *109*, 295−298.

(11) Naguib, M.; Mashtalir, O.; Carle, J.; Presser, V.; Lu, J.; Hultman, L.; Gogotsi, Y.; Barsoum, M. W. Two-Dimensional Transition Metal Carbides. *ACS Nano* **2012**, *6*, 1322−1331.

(12) Kurtoglu, M.; Naguib, M.; Gogotsi, Y.; Barsoum, M. W. First principles study of two-dimensional early transition metal carbides. *MRS Commun.* **2012**, *2*, 133−137.

(13) Halim, J.; Lukatskaya, M. R.; Cook, K. M.; Lu, J.; Smith, C. R.; Naslund, L. A.; May, S. J.; Hultman, L.; Gogotsi, Y.; Eklund, P.; Barsoum, M. W. Transparent Conductive Two-Dimensional Titanium Carbide Epitaxial Thin Films. *Chem. Mater.* **2014**, *26*, 2374−2381.

(14) Hantanasirisakul, K.; Zhao, M. Q.; Urbankowski, P.; Halim, J.; Anasori, B.; Kota, S.; Ren, C. E.; Barsoum, M. W.; Gogotsi, Y. Fabrication of $Ti_3C_2T_x$ MXene Transparent Thin Films with Tunable Optoelectronic Properties. *Adv. Electron Mater.* **2016**, *2*, No. 1600050.

(15) Tang, Q.; Zhou, Z.; Shen, P. W. Are MXenes Promising Anode Materials for Li Ion Batteries? Computational Studies on Electronic Properties and Li Storage Capability of Ti_3C_2 and $Ti_3C_2X_2$ (X = F, OH) Monolayer. *J. Am. Chem. Soc.* **2012**, *134*, 16909−16916.

(16) Xie, Y.; Dall'Agnese, Y.; Naguib, M.; Gogotsi, Y.; Barsoum, M. W.; Zhuang, H. L. L.; Kent, P. R. C. Prediction and Characterization of MXene Nanosheet Anodes for Non-Lithium-Ion Batteries. *ACS Nano* **2014**, *8*, 9606−9615.

(17) Naguib, M.; Halim, J.; Lu, J.; Cook, K. M.; Hultman, L.; Gogotsi, Y.; Barsoum, M. W. New Two-Dimensional Niobium and Vanadium Carbides as Promising Materials for Li-Ion Batteries. *J. Am. Chem. Soc.* **2013**, *135*, 15966−15969.

(18) Dall'Agnese, Y.; Taberna, P. L.; Gogotsi, Y.; Simon, P. Two-Dimensional Vanadium Carbide (MXene) as Positive Electrode for Sodium-Ion Capacitors. *J. Phys. Chem. Lett.* **2015**, *6*, 2305−2309.

DOI: 10.1021/acsomega.7b02001
ACS Omega 2018, 3, 2609−2617

(19) Come, J.; Naguib, M.; Rozier, P.; Barsoum, M. W.; Gogotsi, Y.; Taberna, P. L.; Morcrette, M.; Simon, P. A Non-Aqueous Asymmetric Cell with a Ti_2C-Based Two-Dimensional Negative Electrode. *J. Electrochem. Soc.* **2012**, *159*, A1368−A1373.
(20) Wang, X.; Kajiyama, S.; Iinuma, H.; Hosono, E.; Oro, S.; Moriguchi, I.; Okubo, M.; Yamada, A. Pseudocapacitance of MXene nanosheets for high-power sodium-ion hybrid capacitors. *Nat. Commun.* **2015**, *6*, No. 6544.
(21) Ying, Y.; Liu, Y.; Wang, X. Y.; Mao, Y. Y.; Cao, W.; Hu, P.; Peng, X. S. Two-Dimensional Titanium Carbide for Efficiently Reductive Removal of Highly Toxic Chromium(VI) from Water. *ACS Appl. Mater. Interfaces* **2015**, *7*, 1795−1803.
(22) Peng, Q.; Guo, J. X.; Zhang, Q. R.; Xiang, J. Y.; Liu, B. Z.; Zhou, A. G.; Liu, R. P.; Tian, Y. J. Unique Lead Adsorption Behavior of Activated Hydroxyl Group in Two-Dimensional Titanium Carbide. *J. Am. Chem. Soc.* **2014**, *136*, 4113−4116.
(23) Ren, C. E.; Hatzell, K. B.; Alhabeb, M.; Ling, Z.; Mahmoud, K. A.; Gogotsi, Y. Charge- and Size-Selective Ion Sieving Through Ti_3C_2Tx MXene Membranes. *J. Phys. Chem. Lett.* **2015**, *6*, 4026−4031.
(24) Wang, F.; Yang, C. H.; Duan, C. Y.; Xiao, D.; Tang, Y.; Zhu, J. F. An Organ-Like Titanium Carbide Material (MXene) with Multilayer Structure Encapsulating Hemoglobin for a Mediator-Free Biosensor. *J. Electrochem. Soc.* **2015**, *162*, B16−B21.
(25) Liu, H.; Duan, C. Y.; Yang, C. H.; Shen, W. Q.; Wang, F.; Zhu, Z. F. A novel nitrite biosensor based on the direct electrochemistry of hemoglobin immobilized on MXene-Ti_3C_2. *Sens. Actuators, B* **2015**, *218*, 60−66.
(26) Hu, Q.; Sun, D. D.; Wu, Q. H.; Wang, H. Y.; Wang, L. B.; Liu, B. Z.; Zhou, A. G.; He, J. L. MXene: A New Family of Promising Hydrogen Storage Medium. *J. Phys. Chem. A* **2013**, *117*, 14253−14260.
(27) Khazaei, M.; Arai, M.; Sasaki, T.; Estili, M.; Sakka, Y. Two-dimensional molybdenum carbides: potential thermoelectric materials of the MXene family. *Phys. Chem. Chem. Phys.* **2014**, *16*, 7841−7849.
(28) Ling, Z.; Ren, C. E.; Zhao, M. Q.; Yang, J.; Giammarco, J. M.; Qiu, J. S.; Barsoum, M. W.; Gogotsi, Y. Flexible and conductive MXene films and nanocomposites with high capacitance. *Proc. Natl. Acad. Sci. U.S.A.* **2014**, *111*, 16676−16681.
(29) Chen, J.; Chen, K.; Tong, D. Y.; Huang, Y. J.; Zhang, J. W.; Xue, J. M.; Huang, Q.; Chen, T. CO2 and temperature dual responsive "Smart" MXene phases. *Chem. Commun.* **2015**, *51*, 314−317.
(30) Naguib, M.; Saito, T.; Lai, S.; Rager, M. S.; Aytug, T.; Paranthaman, M. P.; Zhao, M. Q.; Gogotsi, Y. Ti3C2Tx (MXene)-polyacrylamide nanocomposite films. *RSC Adv.* **2016**, *6*, 72069−72073.
(31) Late, D. J. Temperature Dependent Phonon Shifts in Few-Layer Black Phosphorus. *ACS Appl. Mater. Interfaces* **2015**, *7*, 5857−5862.
(32) Su, L. Q.; Zhang, Y. Temperature coefficients of phonon frequencies and thermal conductivity in thin black phosphorus layers. *Appl. Phys. Lett.* **2015**, *107*, No. 071905.
(33) Li, K. L.; Ang, K. W.; Lv, Y. M.; Liu, X. K. Effects of Al2O3 capping layers on the thermal properties of thin black phosphorus. *Appl. Phys. Lett.* **2016**, *109*, No. 261901.
(34) Balandin, A. A.; Ghosh, S.; Bao, W. Z.; Calizo, I.; Teweldebrhan, D.; Miao, F.; Lau, C. N. Superior thermal conductivity of single-layer graphene. *Nano Lett.* **2008**, *8*, 902−907.
(35) Yan, R.; Simpson, J. R.; Bertolazzi, S.; Brivio, J.; Watson, M.; Wu, X. F.; Kis, A.; Luo, T. F.; Walker, A. R. H.; Xing, H. G. Thermal Conductivity of Monolayer Molybdenum Disulfide Obtained from Temperature-Dependent Raman Spectroscopy. *ACS Nano* **2014**, *8*, 986−993.
(36) Calizo, I.; Balandin, A. A.; Bao, W.; Miao, F.; Lau, C. N. Temperature dependence of the Raman spectra of graphene and graphene multilayers. *Nano Lett.* **2007**, *7*, 2645−2649.
(37) Tesfaye, A. T.; Mashtalir, O.; Naguib, M.; Barsoum, M. W.; Gogotsi, Y.; Djenizian, T. Anodized Ti3SiC2 As an Anode Material for Li-ion Microbatteries. *ACS Appl. Mater. Interfaces* **2016**, *8*, 16670−16676.
(38) Halim, J.; Cook, K. M.; Naguib, M.; Eklund, P.; Gogotsi, Y.; Rosen, J.; Barsoum, M. W. X-ray photoelectron spectroscopy of select multi-layered transition metal carbides (MXenes). *Appl. Surf. Sci.* **2016**, *362*, 406−417.
(39) Zhang, T.; Pan, L. M.; Tang, H.; Du, F.; Guo, Y. H.; Qiu, T.; Yang, J. Synthesis of two-dimensional Ti3C2Tx MXene using HCl plus LiF etchant: Enhanced exfoliation and delamination. *J. Alloys Compd.* **2017**, *695*, 818−826.
(40) Hu, T.; Wang, J. M.; Zhang, H.; Li, Z. J.; Hu, M. M.; Wang, X. H. Vibrational properties of Ti3C2 and Ti3C2T2 (T = O, F, OH) monosheets by first-principles calculations: a comparative study. *Phys. Chem. Chem. Phys.* **2015**, *17*, 9997−10003.

DOI: 10.1021/acsomega.7b02001
ACS Omega 2018, 3, 2609−2617